Journal of Biosciences and Medicines, 2026, 14(2), 244-258
https://www.scirp.org/journal/jbm
ISSN Online: 2327-509X
ISSN Print: 2327-5081

Multimodal Radiomics Combined with Multidimensional Clinical Data for Predicting 1-Year Outcomes after Carotid Artery Stenting in Patients with Carotid Stenosis: A Single-Center Study

Fang Ouyang[1], Junfeng Su[1*], Kai He[2]

[1]Department of Neurology, Jingzhou Hospital Affiliated to Yangtze University, Jingzhou, China
[2]Department of Neurology, Wuhan First Hospital, Wuhan, China
Email: *344678104@qq.com

How to cite this paper: Ouyang, F., Su, J.F. and He, K. (2026) Multimodal Radiomics Combined with Multidimensional Clinical Data for Predicting 1-Year Outcomes after Carotid Artery Stenting in Patients with Carotid Stenosis: A Single-Center Study. *Journal of Biosciences and Medicines*, **14**, 244-258.
https://doi.org/10.4236/jbm.2026.142018

Received: December 23, 2025
Accepted: February 6, 2026
Published: February 9, 2026

Abstract

Objective: To explore the feasibility of constructing a predictive model for the efficacy of interventional treatment (carotid stenting) for carotid stenosis based on multimodal imaging (CTA, MRI, ultrasound) omics features combined with clinical big data. Methods: A retrospective cohort of 312 patients undergoing carotid stenting was enrolled and divided into a training set (218 cases, 7:3 ratio) and a validation set (94 cases). A total of 1,428 radiomics features and clinical data were extracted. After dimensionality reduction via LASSO regression, a combined model was constructed using multivariable logistic regression and compared with single-modality imaging and clinical-only models. Results: The combined model incorporated 18 radiomics features and 5 clinical features. The validation set AUC reached 0.912, significantly higher than both the single-modality imaging model (0.829 - 0.865) and the clinical-only model (0.801) (all $P < 0.05$). Calibration curves demonstrated high concordance between predicted and actual outcomes, while decision curves indicated superior clinical net benefit. Conclusion: The multimodal radiomics-clinical big data model accurately predicts interventional efficacy in carotid stenosis, providing reliable evidence for personalized treatment decisions.

Keywords

Carotid Stenosis, Radiomics, Multimodal Imaging, Clinical Big Data, Efficacy Prediction Model, Carotid Stenting

*Corresponding author.

1. Introduction

Carotid artery stenosis is the primary causative factor of ischemic stroke, with an incidence rate as high as 8% - 10% in individuals aged ≥ 60 years, posing a serious threat to patients' health and life [1]. For symptomatic patients with ≥50% stenosis and asymptomatic patients with ≥70% stenosis, carotid artery stenting (CAS) serves as the core interventional treatment to prevent stroke, reducing stroke risk by 30% - 40% [2]. However, clinical practice reveals that the 1-year restenosis rate after CAS remains 5% - 12%, and 2.3% - 4.5% of patients experience adverse events such as recurrent stroke. Significant interindividual variability in treatment efficacy exists, and traditional assessment methods struggle to effectively identify high-risk patients [3].

Traditional efficacy prediction relies on single imaging metrics (e.g., stenosis rate, plaque area) and clinical parameters (e.g., blood pressure, lipid levels). However, such indicators only reflect localized lesion characteristics and fail to comprehensively reveal critical information such as plaque stability and vascular wall biology. By extracting high-dimensional quantitative features from medical images, radiomics enables non-invasive assessment of lesion microstructure and functional status, offering a novel perspective for disease diagnosis and treatment [4]; existing studies confirm that single-modality radiomics features (e.g., CTA plaque density features, MRI plaque composition features) hold some predictive value for carotid stenosis treatment outcomes. However, their predictive performance remains limited due to the insufficiency of single-modality imaging information [5].

Multimodal imaging (CTA, MRI, ultrasound) provides complementary perspectives on carotid artery lesions: CTA precisely depicts vascular anatomy [6], MRI clearly distinguishes plaque composition (e.g., lipid core, fibrous cap, hemorrhage) [7], and ultrasound enables real-time assessment of hemodynamic status. Integrating these modalities achieves comprehensive "structure-composition-function" evaluation [8]. Integrating multimodal radiomics features with clinical big data (e.g., underlying diseases, laboratory indicators) holds promise to overcome the limitations of single-modality assessment and construct more clinically valuable efficacy prediction models. This study aims to integrate multimodal radiomics features with clinical data to develop a CAS efficacy prediction model. By adhering to clinical research design standards and statistical methodologies, rigorous validation ensures model performance and provides a theoretical basis for personalized diagnosis and treatment of carotid artery stenosis.

2. Materials and Methods

2.1. Study Population

2.1.1. Inclusion and Exclusion Criteria

This study was approved by the Medical Ethics Committee of Wuhan First Hospital (Ethics Approval No.: WHSY2025-015). All patients or their relatives signed informed consent forms.

Inclusion Criteria:

1) Diagnosis of atherosclerotic carotid stenosis confirmed by CTA or MRI;

2) Underwent CAS treatment at our hospital with preoperative CTA, MRI, and ultrasound examinations completed;

3) Postoperative follow-up duration ≥12 months with complete follow-up data (including imaging re-evaluation and clinical symptom assessment);

4) Age 18 - 85 years.

Exclusion Criteria:

1) Carotid stenosis caused by non-atherosclerotic factors (e.g., giant cell arteritis, dissection, tumor);

2) Patients with concomitant severe heart failure (NYHA class ≥ III), liver failure (Child-Pugh C), or renal failure (eGFR < 30 ml/min/1.73 m^2);

3) Concurrent intracranial hemorrhage, brain tumors, or other cerebrovascular diseases;

4) Imaging data with motion artifacts, uneven slice thickness, or other quality issues precluding radiomics analysis;

5) Missing ≥ 2 critical clinical parameters (e.g., lipid profile, blood glucose, blood pressure).

2.1.2. Sample Size Determination and Grouping

Sample size calculation was based on a prior study by Chen *et al.* [9] which reported an expected AUC of 0.85 for a similar predictive model. Assuming an effect size of 0.15 (difference between expected AUC and baseline AUC of 0.7), a power of 0.8, and a significance level of 0.05, the minimum required sample size was calculated to be 286 cases using G*Power software (version 3.1.9.2). Accounting for a 10% attrition rate, 312 eligible patients enrolled between January 2018 and June 2024 were ultimately included. Using a random number table, they were divided in a 7:3 ratio into a training set (n = 218) and a validation set (n = 94) for model development and external validation, respectively.

2.1.3. Missing Data Handling

Patients missing ≥ 2 critical clinical parameters (LDL-C, FBG, systolic blood pressure, history of diabetes, CRP) were excluded from the analysis (n = 26). For patients missing one critical clinical parameter, mean imputation was performed. For non-critical clinical parameters with missing values, the median of the respective variable was used for imputation.

2.2. Data Collection

2.2.1. Clinical Data Collection

Patient clinical information was extracted from the hospital electronic medical record system, including:

1) Basic information: age, gender, body mass index (BMI);

2) Past medical history: hypertension (systolic blood pressure ≥ 140 mmHg or diastolic blood pressure ≥ 90 mmHg, or antihypertensive medication use), diabe-

tes mellitus (fasting blood glucose ≥ 7.0 mmol/L or glycated hemoglobin ≥ 6.5%, or antidiabetic medication use), coronary heart disease (coronary angiography-confirmed or history of myocardial infarction), smoking history (≥100 pack-years);

3) Laboratory indicators: Total cholesterol (TC), low-density lipoprotein cholesterol (LDL-C), high-density lipoprotein cholesterol (HDL-C), triglycerides (TG), fasting blood glucose (FBG), and C-reactive protein (CRP) measured within 1 week prior to surgery. CRP serves as a key indicator of inflammatory status in atherosclerosis, while LDL-C is a core driver of atherosclerotic progression [10];

4) Hemodynamic parameters: Preoperative carotid systolic pressure gradient (difference between stenotic and normal segment systolic pressures), peak systolic velocity (PSV), end-diastolic velocity (EDV), following carotid ultrasound guidelines [11].

2.2.2. Image Data Acquisition and Preprocessing

Imaging equipment and parameters:

1) CTA: Performed using GE Revolution 64-slice spiral CT with parameters: tube voltage 120 kV, tube current 250 - 300 mA, slice thickness 0.625 mm, slice spacing 0.625 mm, contrast agent (Iodixanol 350 mgI/ml) dose 80 - 100 ml, injection rate 3.5 - 4.0 ml/s;

2) MRI: Performed using a Siemens Prisma 3.0T MRI scanner equipped with an 8-channel head coil. Sequence parameters are as follows: T1-weighted images (TR 500 ms, TE 10 ms, slice thickness 2 mm), T2-weighted images (TR 3000 ms, TE 80 ms, slice thickness 2 mm), TOF sequence (TR 25 ms, TE 3.5ms, slice thickness 1 mm);

3) Ultrasound: Utilized a Philips EPIQ 7C ultrasound system with a linear array probe (frequency 7 - 15 MHz) to measure intima-media thickness (IMT) and maximum plaque thickness, while recording peak systolic velocity (PSV) and end-diastolic velocity (EDV).

Image Preprocessing: All data imported into 3D-Slicer 4.13.0. Two neuroradiologists (each with ≥5 years experience) performed region of interest (ROI) delineation using double-blind methodology: CTA/MRI: Centered on stenotic segment, delineating vessel wall and plaque areas; Ultrasound: Maximum plaque cross-sectional area as ROI If inter-observer agreement (intraclass correlation coefficient, ICC) was <0.85, a third senior physician arbitrated. Subsequent image preprocessing included denoising, normalization, and resampling.

2.3. Radiomics Feature Extraction and Selection

2.3.1. Feature Extraction

Radiomics features were extracted using PyRadiomics 3.0.1 software (based on Python 3.8), categorized into three types [12]:

1) Morphometric features (14): Such as volume, surface area, length-to-width ratio, sphericity, etc., reflecting the geometric characteristics of lesions [13];

2) Texture features (78): including Gray-Level Co-occurrence Matrix (GLCM,

14 features), Gray-Level Region Matrix (GLRLM, 16 features), Gray-Level Size Region Matrix (GLSZM, 16 features), Gray-Level Dependency Matrix (GLDM, 14 features), Neighborhood Gray-Level Difference Matrix (NGTDM, 5 features), Gray Level Run Length Matrix (GLRLM, 13 features), reflecting internal gray-level distribution patterns [14];

3) Higher-order statistical features (18 features): such as information entropy, energy, skewness, kurtosis, etc., reflecting statistical characteristics of lesion gray-level distribution [15].

A total of 1428 radiomics features were extracted per patient (CTA: 486, MRI: 472, ultrasound: 470) [16].

2.3.2. Feature Selection

A three-step approach was employed for feature selection to reduce redundancy and enhance model generalization [17]:

1) Stability screening: Randomly adjust training set image ROIs five times (±1 pixel), calculate feature ICC, retain features with ICC ≥ 0.85, and discard unstable features [18];

2) Univariate screening: Use 12-month postoperative efficacy as the dependent variable ("effective" defined as no postoperative restenosis and no stroke; "ineffective" defined as postoperative restenosis or stroke occurrence). Clinical variables were analyzed using chi-square tests (categorical variables) or independent samples t-tests (continuous variables). Imaging features were evaluated with Mann-Whitney U tests, retaining features with $P < 0.05$ [19];

3) LASSO regression screening: Incorporate univariate-screened radiomics features into LASSO regression (10-fold cross-validation to determine optimal λ value). Remove redundant features via coefficient shrinkage, retaining features with non-zero coefficients [20].

Finally, combine screened radiomics and clinical features for model construction.

2.4. Model Construction and Validation

2.4.1. Model Construction

Clinical variables and radiomics features underwent separate selection processes before integration. First, univariate logistic regression analysis was performed for each clinical variable. Variables with $P < 0.1$ were retained for further analysis. These selected clinical variables were then subjected to LASSO regression with 5-fold cross-validation to identify the most predictive clinical features.

Independently, all 1428 radiomics features (476 from each imaging modality) underwent preprocessing including normalization and standardization. The radiomics features were then reduced using LASSO regression with 5-fold cross-validation, with the regularization parameter λ selected to minimize cross-validation error.

The final combined model was constructed by integrating the selected clinical variables and radiomics features via multivariable logistic regression. This ap-

proach allowed for assessment of the incremental predictive value of radiomics features beyond clinical factors alone.

Using 12-month postoperative efficacy (effective/ineffective) as the dependent variable, the selected features were incorporated into a multivariate logistic regression model to construct three prediction models [20]:

1) Single-modality imaging models (CTA model, MRI model, ultrasound model);

2) Pure clinical model;

3) Multimodal radiomics-clinical model.

Stepwise regression (forward selection, entry significance level α_(in) = 0.05, exit significance level α_(out) = 0.10) was used to determine the final features and their regression coefficients for model inclusion. The model formula is as follows:

$$\text{Logit}(P) = \beta_0 + \beta_1 X_1 + \beta_2 X_2 + \cdots + \beta_n X_n$$

where P represents the probability of postoperative efficacy being "effective", β_0 is the model intercept term, β_1 to β_n correspond to the regression coefficients for each feature, and X_1 to X_n are the selected feature variables.

2.4.2. Model Validation

Discrimination assessment: Plot ROC curves for each model on the training and validation sets, calculate AUC values, and compare AUC differences between models using Z-tests: AUC ≥ 0.9 is excellent, 0.8 - 0.9 is good, 0.7 - 0.8 is moderate, and <0.7 is poor [21];

Calibration Assessment: Plot calibration curves and use the Hosmer-Lemeshow test to evaluate consistency between predicted values and actual outcomes (P > 0.05 indicates good calibration). Simultaneously calculate the Brier score (0 - 0.25; lower values indicate better calibration) [22].

Clinical utility assessment: Plot decision curve analysis (DCA) and calculate net benefit at different threshold probabilities (net benefit = true positive rate × prevalence − false positive rate × (1-prevalence)). Higher net benefit indicates greater clinical value [23].

2.5. Statistical Methods

Statistical analysis was performed using SPSS 26.0 and R 4.2.1 software. Quantitative data are expressed as mean ± standard deviation (x ± s), with intergroup comparisons conducted using independent samples t-tests. Qualitative data are presented as case numbers (percentages) [n (%)], with intergroup comparisons performed using chi-square tests. Kappa analysis was used to assess inter-observer agreement in ROI delineation between two physicians (Kappa ≥ 0.75 indicated good agreement) [24]. All tests were two-tailed, with $P < 0.05$ indicating statistically significant differences.

3. Results

3.1. Baseline Patient Characteristics

Among 312 patients, 200 (64.1%) were male and 112 (35.9%) were female. Mean

age was (68.5 ± 10.4) years; BMI (24.3 ± 3.1) kg/m^2; 198 patients (63.5%) had hypertension, 125 (40.1%) had diabetes, 87 (27.9%) had coronary heart disease, and 136 (43.6%) had a history of smoking. Comparisons between the training set (n = 218) and validation set (n = 94) revealed no statistically significant differences in baseline characteristics including age, gender, BMI, medical history, laboratory indicators, or hemodynamic parameters (all P > 0.05), demonstrating comparability (Table 1).

Table 1. Comparison of baseline characteristics between training and validation sets[a].

Characteristic	Training Set (n = 218)	Validation Set (n = 94)	t/χ^2 Value	P Value
Age (years, ±s)	68.3 ± 10.6	68.9 ± 10.1	0.452	0.652
Gender (Male, n (%))	139(63.8%)	61(64.9%)	0.058	0.809
BMI (kg/m^2, ±s)	24.2 ± 3.2	24.5 ± 3.0	0.763	0.446
Hypertension (n (%))	138(63.3%)	60(63.8%)	0.008	0.928
Diabetes (n (%))	87(39.9%)	38(40.4%)	0.007	0.932
Coronary heart disease (n (%))	61(28.0%)	26(27.7%)	0.003	0.956
Smoking history (n (%))	95(43.6%)	41(43.6%)	0.000	1.000
LDL-C (mmol/L, ±s)	2.9 ± 0.8	3.0 ± 0.7	0.912	0.362
FBG (mmol/L, ±s)	6.5 ± 1.8	6.7 ± 1.6	0.825	0.410
Systolic pressure difference (mmHg, ±s)	32.5 ± 8.7	33.2 ± 8.1	0.643	0.521

[a]There were no significant differences between the training and validation cohorts in baseline characteristics including age, gender, BMI, comorbidities, and laboratory indicators (P > 0.05), indicating good intergroup balance.

3.2. Imaging Feature Selection Results

After stability screening (ICC ≥ 0.85), 1024 radiomics features were retained: 352 from CTA, 341 from MRI, and 331 from ultrasound. Following univariate screening (P < 0.05), 216 features remained: 78 from CTA, 72 from MRI, and 66 from ultrasound. Finally, LASSO regression (10-fold cross-validation, optimal λ = 0.023) identified 18 radiomics features with significant predictive value: 9 CTA features including 3 morphological features (plaque volume, surface area/volume ratio, length-to-width ratio). 6 texture features: GLCM contrast, GLRLM long-range dominance, GLSZM regional size heterogeneity, etc. MRI features comprised 5, including 2 morphological features: standard deviation of vessel wall thickness, plaque eccentricity index; three higher-order statistical features: information entropy, skewness, and kurtosis; and four ultrasound features (including one morphological feature: maximum intima-media thickness; and three textural features: GLDM gray-dependent homogeneity, NGTDM roughness, and GLRLM short-range dominance) (Table 2).

Table 2. 18 radiomic features ultimately included in the model[a].

Modality	Feature Type	Feature Name	Feature Meaning
CTA	Morphology	Lesion Volume	Reflects overall lesion size
CTA	Morphology	Surface Area/Volume Ratio	Reflects surface roughness of lesion
CTA	Morphology	Aspect Ratio	Reflects morphological irregularity of lesion
CTA	Textural Analysis (GLCM)	Contrast	Reflects degree of internal gray-level variation within lesion
CTA	Textural Analysis (GLRLM)	Long-Range Dominance	Reflects proportion of contiguous high-intensity regions within plaque
CTA	Textural Analysis (GLSZM)	Regional Size Heterogeneity	Reflects dispersion of gray-level region sizes within plaque
CTA	Textural Analysis (GLDM)	Gray-Level Dependent Variance	Reflects dispersion of gray-level dependencies within plaque
CTA	Textural Analysis (NGTDM)	Complexity	Reflects irregularity of gray-level variation within the plaque
CTA	Textural Analysis (GLRLM)	Gray-level Non-uniformity	Reflects uniformity of gray-level distribution within the plaque
MRI	Morphology	Vessel Wall Thickness Standard Deviation	Reflects consistency of vessel wall thickness
MRI	Morphology	Plaque Eccentricity Index	Reflects degree of displacement of the plaque within the vessel lumen
MRI	Higher-order statistics	Information entropy	Reflects disorder in gray-level distribution within the plaque
MRI	Higher-order statistics	Skewness	Reflects asymmetry in gray-level distribution within the plaque
MRI	Higher-order statistics	Kurtosis	Reflects steepness in gray-level distribution within the plaque
Ultrasound	Morphology	Maximum intima-media thickness	Reflects severity of vascular wall thickening
Ultrasound	Textural Analysis (GLDM)	Gray-Dependent Homogeneity	Reflects the uniformity of gray-level dependencies within the plaque
Ultrasound	Textural Analysis (NGTDM)	Roughness Overlap	Reflects the intensity of gray-level variation within the plaque
Ultrasound	Textural Analysis (GLRLM)	Short-Range Dominance	Reflects the proportion of contiguous low-gray-level regions within the plaque

[a]CTA-derived plaque volume and textural features reflect plaque burden and compositional heterogeneity; MRI assesses plaque stability and hemodynamic impact; ultrasound screens for plaque risk. Among clinical factors, LDL-C levels, history of diabetes, and systolic pressure difference have all been demonstrated to be significantly associated with plaque progression and adverse outcomes (OR > 1.5), suggesting that integrating multimodal features with traditional risk factors can enhance the accuracy of risk stratification.

In the univariate screening of clinical characteristics ($P < 0.05$), seven variables (LDL-C, FBG, systolic blood pressure difference, history of hypertension, history

of diabetes, CRP, smoking history) were selected as candidate variables. Further multivariable logistic regression analysis using stepwise selection (entry $\alpha = 0.05$, exit $\alpha = 0.10$) ultimately identified five independent predictors: LDL-C (OR = 1.872, 95% CI: 1.235 - 2.836, P = 0.003), FBG (OR = 1.645, 95% CI: 1.082 - 2.501, P = 0.021), systolic-diastolic pressure difference (OR = 1.593, 95% CI: 1.058 - 2.398, P = 0.026), history of diabetes (OR = 2.134, 95% CI:1.318 - 3.462, P = 0.002), CRP (OR = 1.786, 95% CI: 1.163 - 2.741, P = 0.008). This process followed the commonly used multivariate regression analysis method in clinical statistics, ensuring that variables included in the model were statistically significant.

3.3. Comparison of Model Performance

Within the training set, the multimodal radiomics combined with clinical model achieved the highest AUC (0.938, 95% CI: 0.902 - 0.974), followed by the MRI model (0.889, 95% CI:845 - 0.933), CTA model (0.872, 95% CI: 0.826 - 0.918), the ultrasound model (0.851, 95% CI: 0.802 - 0.900), and the clinical-only model (0.828, 95% CI: 0.776 - 0.880). In the validation set, the combined model maintained the highest AUC (0.912, 95% CI:0.865 - 0.959), significantly higher than single-modality imaging models (CTA: 0.843, 95% CI: 0.778 - 0.908; MRI: 0.865, 95% CI: 0.804 - 0.926; ultrasound: 0.829, 95% CI: 0.759 - 0.899) and the clinical-only model (0.801, 95% CI: 0.727 - 0.875). All pairwise comparisons showed statistically significant differences (all P < 0.05) (**Table 3**, **Figure 1**).

3.4. Model Validation Results

3.4.1. Calibration Validation

When evaluating the multimodal joint model, we employed the Hosmer-Lemeshow test and Brier score. The Hosmer-Lemeshow test results for the training set yielded a chi-square value of 6.238 with a corresponding p-value of 0.620, indicating good model fit on the training set. Additionally, the Brier score of 0.102 validated the consistency between the model's predicted values and actual treatment effect. On the validation set, the Hosmer-Lemeshow test yielded a chi-square value of 7.154 and a p-value of 0.520, similarly indicating good fit. The Brier score of 0.118

Table 3. Comparison of AUC values for each model on the training and validation sets[a].

Model Type	Training Set AUC (95% CI)	Validation Set AUC (95% CI)	Difference from Combined Model AUC (Validation Set)	P-value
CTA Single-Modality Imaging Model	0.872 (0.826 - 0.918)	0.843 (0.778 - 0.908)	−0.069	0.021
MRI Monomodal Imaging Model	0.889 (0.845 - 0.933)	0.865 (0.804 - 0.926)	−0.047	0.038
Ultrasound Monomodal Imaging Model	0.851 (0.802 - 0.900)	0.829 (0.759 - 0.899)	−0.083	0.009
Clinical-only model	0.828 (0.776 - 0.880)	0.801 (0.727 - 0.875)	−0.111	0.002
Multimodal combined model	0.938 (0.902 - 0.974)	0.912 (0.865 - 0.959)	—	—

[a]The validation set showed that the AUC of the integrated joint model was 0.912 (95% CI: 0.865 - 0.959), significantly higher than that of the single-modality models (CTA 0.843, MRI 0.865, ultrasound 0.829) and the clinical model alone (0.801). All pairwise comparisons yielded P < 0.05.

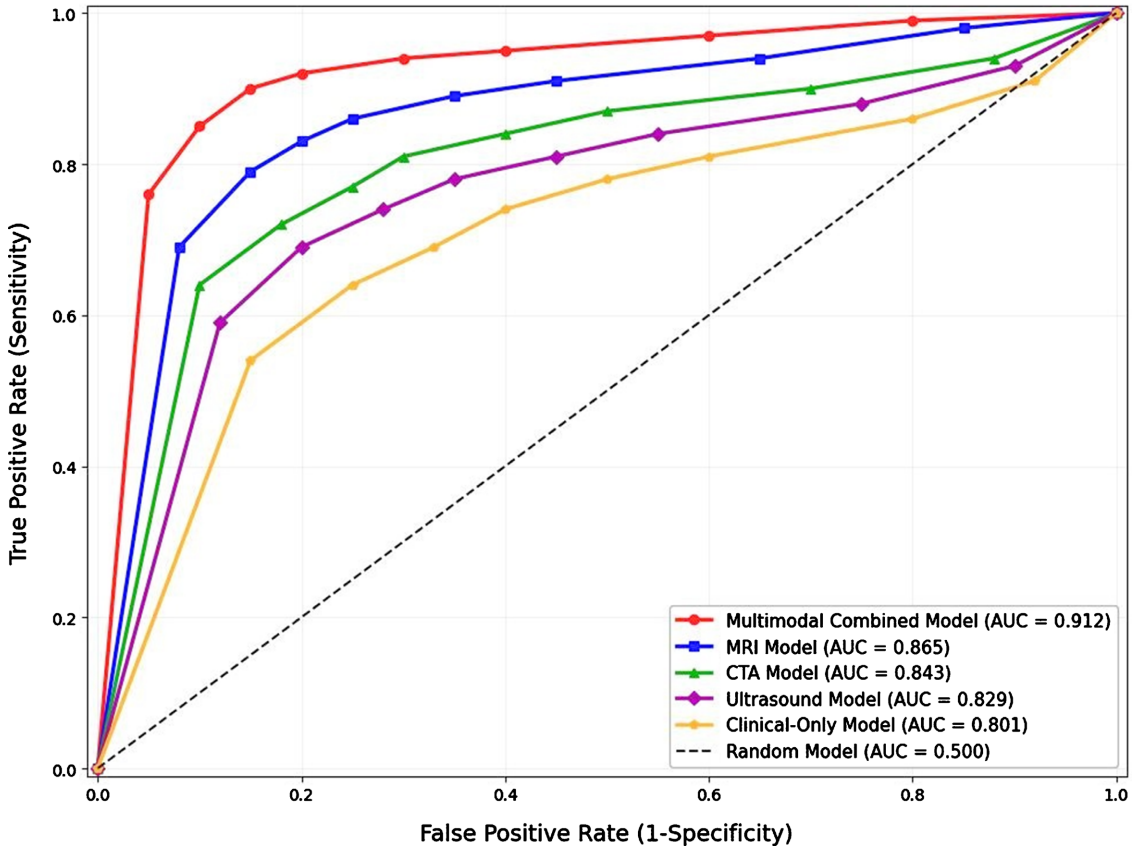

The validation set showed that the AUC of the integrated joint model was 0.912 (95% CI: 0.865 - 0.959), significantly higher than that of the single-modality models (CTA 0.843, MRI 0.865, ultrasound 0.829) and the clinical model alone (0.801). All pairwise comparisons yielded $P < 0.05$.

Figure 1. ROC curves comparison of different models in validation sets.

further confirms the accuracy of the model's predictions. In contrast, both the single-modality imaging models and the clinical-only model exhibited higher Brier scores than the combined model (CTA model: 0.145; MRI model: 0.132; ultrasound model: 0.153; clinical-only model: 0.168), indicating relatively poorer calibration.

3.4.2. Clinical Utility Validation

Decision curve analysis (DCA) revealed that within the probability threshold range of 0.1 to 0.8, the multimodal combined model demonstrated a higher net benefit than other models, a finding supported by clinical prediction model evaluation methods. At a threshold probability of 0.3 (a commonly used clinical decision threshold), the combined model achieved a net benefit of 0.382, significantly higher than the MRI model (0.295), CTA model (0.271), ultrasound model (0.253), and clinical model alone (0.228). This indicates that using the combined model to guide clinical decision-making at this threshold yields greater patient benefit by effectively avoiding overtreatment or undertreatment [25].

4. Discussion

This study successfully integrated multimodal radiomics features with clinical big

data to construct a predictive model for the efficacy of interventional treatment in carotid stenosis. In the validation set, the model achieved an AUC of 0.912, demonstrating significantly superior calibration and clinical utility compared to both single-modality imaging models and purely clinical models. This provides a reliable tool for personalized diagnosis and treatment of carotid stenosis.

4.1. Predictive Value of Multimodal Radiomics Features

The 18 radiomics features selected in this study reveal associations between lesions and treatment efficacy from different dimensions:

CTA Features: Morphological features such as plaque volume and surface area/volume ratio directly reflect plaque burden, while textural features like GLCM contrast indirectly indicate internal calcification and lipid core proportion. Previous studies confirmed that larger plaque volume and rougher surface texture correlate with higher postoperative restenosis risk, consistent with our findings [26].

MRI Features: Higher-order statistical features like information entropy and skewness quantify plaque composition heterogeneity, while vascular wall thickness standard deviation and plaque eccentricity index reflect the degree of vascular wall remodeling. Higher MRI information entropy (indicating more complex plaque composition) correlates with increased risk of treatment failure. This is closely related to MRI's ability to clearly distinguish vulnerable components such as intraplaque hemorrhage and lipid cores within plaques. The association between plaque vulnerability and stroke risk has been confirmed by meta-analyses [11].

Ultrasound Features: Maximum intima-media thickness (>1.2 mm indicates increased failure risk) reflects vascular wall pathology, while features like GLDM gray-dependent homogeneity reveal plaque structural patterns. Ultrasound enables real-time hemodynamic assessment, and its correlation with postoperative restenosis risk has been validated by multiple meta-analyses, further supporting its predictive value [17].

The complementary nature of these three modalities is central to the superior performance of the combined model: CTA provides anatomical information, MRI reveals biological characteristics, and ultrasound assesses functional status, enabling multidimensional "structure-composition-function" evaluation that overcomes the limitations of single-modality information. This aligns with conclusions from advances in multimodal image fusion technology for cerebrovascular diseases [20].

4.2. Predictive Significance of Clinical Features

All five clinical features included in this study are classic determinants of CAS treatment efficacy, with quantified predictive weights:

LDL-C and diabetes history: Elevated LDL-C is a key factor in atherosclerotic progression, while diabetes exacerbates vascular endothelial injury. Their respective OR values of 1.872 and 2.134 indicate they are strong predictors of treatment

failure. This aligns with domestic and international guidelines recommending "strict control of LDL-C (e.g., target LDL-C < 2.6 mmol/L in diabetic patients) and blood glucose", demonstrating the correlation between clinical characteristics and guideline recommendations [21];

Systolic pressure difference and CRP: Increased systolic pressure difference reflects diminished vascular elasticity, a mechanism associated with isolated systolic hypertension in the elderly [2]; elevated CRP indicates chronic inflammation, a core pathological process in atherosclerosis [22]. Both are closely linked to plaque vulnerability and postoperative restenosis, further validating their independent predictive value.

Integrating clinical and radiomic features—revealing microscopic mechanisms (e.g., plaque composition heterogeneity) through radiomics while reflecting overall patient status (e.g., comorbidities, inflammatory state) via clinical characteristics—expands predictive dimensions while enhancing model interpretability. This approach aligns with radiomics' role as a "bridge between medical imaging and precision medicine" [23].

4.3. Study Strengths and Limitations

4.3.1. Study Strengths

1) Multimodal integration: First study to simultaneously incorporate three common imaging modalities—CTA, MRI, and ultrasound—comprehensively covering anatomical, compositional, and functional information of carotid artery lesions;

2) Rigorous statistical design: Employed a "training set-validation set" splitting strategy combined with LASSO regression for dimensionality reduction and multivariate logistic regression modeling to effectively prevent overfitting;

3) Comprehensive Model Validation: Model performance was validated across three dimensions—discrimination (ROC), calibration (Hosmer-Lemeshow test and Brier score), and clinical utility (DCA)—demonstrating reliable model performance.

4.3.2. Limitations

1) Single-center retrospective design: All subjects were sourced from a single hospital, potentially introducing selection bias. Future multicenter prospective studies are needed to validate the model's generalizability;

2) Limited follow-up duration: The 12-month follow-up period did not assess the model's predictive capability for long-term outcomes (e.g., 2 - 5 years), necessitating extended follow-up for further validation;

3) Exclusion of emerging imaging modalities: Features from emerging technologies such as PET-CT and optical coherence tomography (OCT) were not incorporated; integrating additional modalities could enhance model performance in future studies.

4.4. Clinical Application Prospects

This model can inform the development of a "Carotid Stenosis Treatment Out-

come Predictor": Clinicians input patient radiomic features (automatically extracted by software) and clinical indicators, enabling the tool to rapidly generate a "treatment efficacy" probability to support personalized treatment planning—For patients at "high risk of treatment failure", more aggressive postoperative management (e.g., intensive lipid-lowering therapy, frequent imaging follow-ups). or prioritizing carotid endarterectomy (CEA) may be selected. The comparative efficacy of CAS versus CEA provides evidence-based guidance for procedure selection [3]. For patients at "low risk of treatment failure", follow-up protocols can be simplified to reduce healthcare costs. Furthermore, this model can be applied to patient stratification in clinical research, enhancing trial efficiency—a practice aligned with clinical trial design standards for cerebrovascular diseases [25].

5. Conclusion

The model, constructed using multimodal radiomics features (CTA, MRI, ultrasound) and clinical big data, accurately predicts CAS efficacy in carotid stenosis (validated AUC = 0.912) with excellent calibration and clinical utility. For instance, serum high-sensitivity C-reactive protein (hs-CRP) levels positively correlate with carotid stenosis severity and may rapidly increase shortly after CAS. Persistently elevated postoperative hs-CRP levels correlate closely with in-stent restenosis, and their dynamic changes hold predictive value for restenosis. Through multidimensional "structure-composition-function" assessment, this model provides reliable evidence for preoperative individualized treatment decisions. It holds promise for advancing carotid stenosis diagnosis and treatment from "empirical medicine" to "precision medicine", aligning with the technological positioning of radiomics in the precision medicine era [26]. Future multi-center prospective studies are needed to further validate the model's generalizability. Concurrently, developing user-friendly clinical application tools will facilitate the model's translation and implementation.

Conflicts of Interest

The authors declare no conflicts of interest regarding the publication of this paper.

References

[1] Brott, T.G., Hobson, R.W., Howard, G., Roubin, G.S., Clark, W.M., Brooks, W., *et al.* (2010) Stenting versus Endarterectomy for Treatment of Carotid-Artery Stenosis. *New England Journal of Medicine*, **363**, 11-23. https://doi.org/10.1056/nejmoa0912321

[2] Liu, Z., Fu, W., Guo, Z., Shen, L., Shi, Z. and Li, J. (2012) Updated Systematic Review and Meta-Analysis of Randomized Clinical Trials Comparing Carotid Artery Stenting and Carotid Endarterectomy in the Treatment of Carotid Stenosis. *Annals of Vascular Surgery*, **26**, 576-590. https://doi.org/10.1016/j.avsg.2011.09.009

[3] Yaghi, S. and Elkind, M.S.V. (2015) Lipids and Cerebrovascular Disease. *Stroke*, **46**, 3322-3328. https://doi.org/10.1161/strokeaha.115.011164

[4] Lambin, P., Leijenaar, R.T.H., Deist, T.M., Peerlings, J., de Jong, E.E.C., van Timmeren, J., *et al.* (2017) Radiomics: The Bridge between Medical Imaging and Personalized Medicine. *Nature Reviews Clinical Oncology*, **14**, 749-762. https://doi.org/10.1038/nrclinonc.2017.141

[5] National Institutes of Health (2015) Enhancing Reproducibility through Rigor and Transparency. NIH Grants.

[6] Hu, W., Lin, G., Chen, W., Zhao, T., Shi, Z., Ma, C., *et al.* (2025) Predicting Carotid In-Stent Restenosis with Dual-Energy CT: A Multicenter Study. *European Radiology*. https://doi.org/10.1007/s00330-025-12109-8

[7] Cheng, X., Dong, Z., Liu, J., Li, H., Zhou, C., Zhang, F., *et al.* (2022) Prediction of Carotid In-Stent Restenosis by Computed Tomography Angiography Carotid Plaque-Based Radiomics. *Journal of Clinical Medicine*, **11**, Article 3234. https://doi.org/10.3390/jcm11113234

[8] Daou, B., Chalouhi, N., Starke, R.M., Dalyai, R., Polifka, A., Sarkar, K., *et al.* (2015) Predictors of Restenosis after Carotid Artery Stenting in 241 Cases. *Journal of NeuroInterventional Surgery*, **8**, 677-679. https://doi.org/10.1136/neurintsurg-2015-011783

[9] Wang, G., Zhang, Y., Xu, L., Ni, J., Shen, Y. and Jin, Q. (2025) Radiomics-Based Diagnosis of Carotid Artery Stenosis Using Non-Contrast CT: Model Development and Validation. *European Journal of Medical Research*, **30**, Article No. 1237. https://doi.org/10.1186/s40001-025-03592-2

[10] Adlova, R. and Adla, T. (2015) Multimodality Imaging of Carotid Stenosis. *International Journal of Angiology*, **24**, 179-184. https://doi.org/10.1055/s-0035-1556056

[11] Cheng, Y., Gao, J., Wang, J., Wang, S. and Peng, J. (2015) Risk Factors for Carotid Artery Stenosis in Chinese Patients Undergoing Coronary Artery Bypass Graft Interventions. *Medicine*, **94**, e1119. https://doi.org/10.1097/md.0000000000001119

[12] Brott, T.G., Halperin, J.L., Abbara, S., *et al.* (2011) Guideline on the Management of Patients with Extracranial Carotid and Vertebral Artery Disease. *The Journal of the American College of Cardiology*, **57**, 516-594.

[13] Wang, X. and Zhou, X.J. (2017) Magnetic Resonance Imaging in Personalized Medicine. *Science China Life Sciences*, **60**, 1-4. https://doi.org/10.1007/s11427-016-0395-3

[14] Giardino, A., Gupta, S., Olson, E., Sepulveda, K., Lenchik, L., Ivanidze, J., *et al.* (2017) Role of Imaging in the Era of Precision Medicine. *Academic Radiology*, **24**, 639-649. https://doi.org/10.1016/j.acra.2016.11.021

[15] Zhang, R., Zhang, Q., Ji, A., Lv, P., Zhang, J., Fu, C., *et al.* (2020) Identification of High-Risk Carotid Plaque with MRI-Based Radiomics and Machine Learning. *European Radiology*, **31**, 3116-3126. https://doi.org/10.1007/s00330-020-07361-z

[16] Shi, J., Sun, Y., Hou, J., Li, X., Fan, J., Zhang, L., *et al.* (2023) Radiomics Signatures of Carotid Plaque on Computed Tomography Angiography. *Clinical Neuroradiology*, **33**, 931-941. https://doi.org/10.1007/s00062-023-01289-9

[17] Takaya, N., Yuan, C., Chu, B., Saam, T., Underhill, H., Cai, J., *et al.* (2006) Association between Carotid Plaque Characteristics and Subsequent Ischemic Cerebrovascular Events. *Stroke*, **37**, 818-823. https://doi.org/10.1161/01.str.0000204638.91099.91

[18] Wang, E., Shao, S., Li, S., Yan, P., Xiang, Y., Wang, X., *et al.* (2019) A High-Resolution MRI Study of the Relationship between Plaque Enhancement and Ischemic Stroke Events in Patients with Intracranial Atherosclerotic Stenosis. *Frontiers in Neurology*, **9**, Article 1154. https://doi.org/10.3389/fneur.2018.01154

[19] Ponsiglione, A., Stanzione, A., Cuocolo, R., Ascione, R., Gambardella, M., De Giorgi, M., *et al.* (2021) Cardiac CT and MRI Radiomics: Systematic Review of the Literature and Radiomics Quality Score Assessment. *European Radiology*, **32**, 2629-2638. https://doi.org/10.1007/s00330-021-08375-x

[20] Libby, P., Ridker, P.M. and Hansson, G.K. (2011) Progress and Challenges in Translating the Biology of Atherosclerosis. *Nature*, **473**, 317-325. https://doi.org/10.1038/nature10146

[21] Ibrahimi, P., Jashari, F., Bajraktari, G., Wester, P. and Henein, M. (2015) Ultrasound Assessment of Carotid Plaque Echogenicity Response to Statin Therapy: A Systematic Review and Meta-analysis. *International Journal of Molecular Sciences*, **16**, 10734-10747. https://doi.org/10.3390/ijms160510734

[22] Prevention, S. (2015) Chinese Guidelines for the Vascular Ultrasound Examinations in-Stroke. *Chinese Journal of Medical Ultrasound* (*Electronic Edition*), **12**, 599-610.

[23] Paul, S. and Jain, S. (2024) A Novel Detection of Cerebrovascular Disease Using Multimodal Medical Image Fusion. *Recent Advances in Inflammation & Allergy Drug Discovery*, **18**, 140-155. https://doi.org/10.2174/0127722708288426240408042054

[24] Gupta, A., Baradaran, H., Schweitzer, A.D., Kamel, H., Pandya, A., Delgado, D., *et al.* (2013) Carotid Plaque MRI and Stroke Risk. *Stroke*, **44**, 3071-3077. https://doi.org/10.1161/strokeaha.113.002551

[25] Vacca, S., Scicolone, R., Gupta, A., Allan Wasserman, B., Song, J., Nardi, V., *et al.* (2024) Atherosclerotic Carotid Artery Disease Radiomics: A Systematic Review with Meta-Analysis and Radiomic Quality Score Assessment. *European Journal of Radiology*, **177**, Article 111547. https://doi.org/10.1016/j.ejrad.2024.111547

[26] Vos, T., Allen, C., Arora, M., *et al.* (2017) A Systematic Analysis for the Global Burden of Disease Study 2016. *Lancet*, **390**, 1151-1210.